



1-D Metal-Dielectric-Metal Grating Structure as an Ultra-Narrowband Perfect Plasmonic Absorber in the Visible and Its Application in Glucose Detection

Sandeep Kumar Chamoli^{1,2,3} · Subhash C. Singh^{1,2,3} · Chunlei Guo^{1,2,3}

Received: 26 December 2019 / Accepted: 22 March 2020 / Published online: 4 April 2020
© Springer Science+Business Media, LLC, part of Springer Nature 2020

Abstract

The need for an easy to fabricate perfect and narrowband light absorber in the visible range of electromagnetic (EM) spectrum has always been in demand for many scientific and device applications. Here, we propose a metal-dielectric-metal (MDM) 1-D grating plasmonic structure as a perfect narrow band light absorber in the visible and its application in glucose detection. The proposed structure consists of a 1- D grating of gold on the top of a dielectric layer on a gold film. Optimization for dielectric grating index (n), grating thickness (t), grating width (W), and grating period (P) has been done to improve the performance of plasmonic structure by calculating its quality factor and figure-of-merit (FOM). The optimized plasmonic structure behaves as a perfect narrowband light absorber. The flexibility to work at a specific wavelength is also offered by the proposed structure through an appropriate selection of the geometrical parameters and refractive index of the dielectric grating. The equivalent RC model is used to understand different components of the proposed structure on the optical response. The absorption response of the structure is invariant to the incident angle. Moreover, the calculated absorbance of the proposed plasmonic structure is $\sim 100\%$ with a narrow full-width half maxima (FWHM) of ~ 2.8 nm. We have numerically demonstrated a potential application of the proposed MDM absorber as a plasmonic glucose sensor in the visible range with detection sensitivity in the range of 140 to 195 nm/RIU.

Keywords Optical sensors · Plasmons · Optical detectors · Glucose detection · Metal-dielectric-metal · LC equivalent circuit

Introduction

Recently, plasmonic metamaterials have attracted significant research interest due to their ability to control, alter, and magnify properties of incident electromagnetic radiation. These surfaces have promising applications in confining light in

sub-wavelength dimensions [1–3], in enhanced light transmission [4, 5], in optical couplers and waveguides [6], in optical sensing [1, 6], and so on. Moreover, plasmonic metamaterials have been recently used in photonic modulators [7–9], photodetectors [10, 11], thermal imaging [12], microbolometers [13], and so on. It has always been beneficial to enhance plasmonic absorption for the compensation of intrinsic optical losses of metals in an efficient plasmonic system. Based on their applications, plasmonic absorption is classified into two categories namely broadband absorption and narrowband absorption. Broadband plasmonic absorbers have applications in solar-thermal energy harvesting [14, 15] and broadband photodetection [16], while narrowband plasmonic absorbers are applicable in narrow-band rejection optical filters, plasmonic SERS sensing [17, 18], and monochromatic photodetection [19, 20]. Research in the field of perfect plasmonic metamaterial absorption is rapidly increasing after its first demonstration in 2008 by N.I. Landy [21]. Generally, an array of discretely placed sub-wavelength resonators over plasmonic metamaterial surfaces are required to absorb

✉ Subhash C. Singh
ssingh49@ur.rochester.edu

✉ Chunlei Guo
guo@optics.rochester.edu

¹ The Guo China-US Photonics Laboratory, State Key Laboratory of Applied Optics, Changchun Institute of Optics, Fine Mechanics and Physics, Chinese Academy of Sciences, University of Chinese Academy of Science, Changchun 130033, China

² University of Chinese Academy of Science, Beijing 100039, China

³ The Institute of Optics, University of Rochester, Rochester, NY 14627, USA

electromagnetic radiation in the visible and near-infrared spectral range [22–24].

A blackbody is considered a perfect broadband absorber with an ability to absorb all electromagnetic radiation incident on it. However, it is challenging to realize a perfect light absorption in a narrowband spectral region. Due to the generation of surface plasmons at the metal-dielectric interface, a huge enhancement in the electric field on their surface can be observed. A conventional approach to design a metal-dielectric-metal (MDM) plasmonic absorber generally consists of three layers. The uppermost layer consists of a periodic metal structure or grating, the third (lowest) layer is the same metal film, and a thin dielectric layer is sandwiched between top metallic structure and bottom metal film [17–23]. The uppermost periodic grating metal layer follows impedance matching criteria and behaves like an electric resonator that supervises electric field response of the corresponding structure [23, 24]. The sandwiched dielectric layer plays an important role in determining the position of perfect absorption and works as a light absorber layer. However, the lower metal film with a thickness larger than the light penetration depth works as a reflector layer to reduce light transmission. Several MDM-based plasmonic absorbers have been designed and proposed by researchers to attain perfect light absorption where most of the studies are based on the design of upper metallic structures such as stripe, ellipse, circle, rectangular, and U-shaped periodic patterns. Yu et al. proposed a four-layer metamaterial absorber where the sequence of layers is as follows from top to down: metallic rings, dielectric spacer, metal film, and the silicon substrate. They achieved two distinct narrow absorption bands in the range 3–5 μm and 8–14 μm by optimizing the radius of the gold ring and refractive index. The maximum absorption achieved by two peaks was 95.1% [25]. Wang et al. proposed four-band and polarization-insensitive metamaterial absorber in the near-infrared with maximum absorption of 97%. The structure consists of four layers in the following manner from top to down: four metallic square rings, dielectric spacer, and metal film at the bottom [26]. Dayal et al. introduced a metal-dielectric stacked metamaterial absorber in the infrared region and reported three absorption bands. The designed structure was able to attain a peak absorption of 98% [27]. Tao et al. suggested a three-layer dual-band absorber in the terahertz region. The top and the bottom metallic layers are separated by a dielectric layer. The first peak was at 1.4 THz with 85% absorption and the second peak was at 3.0 THz with 94% peak absorption.

In plasmonic sensing, a narrowband perfect absorber with the position of resonance absorbance highly sensitive to the ambient refractive index is required. In the past, several experimental and theoretically strategies were implemented to realize plasmonic sensing in infrared and terahertz spectral regions of electromagnetic radiation [28, 29]. However, due to the unavailability of low-cost light sources [30] and photodetectors in infrared and

terahertz spectral regions, it is not viable to fabricate low-cost plasmonic sensors for immediate point of care in underdeveloped countries. In contrast, the availability of low-cost, but high-value coherent and non-coherent light sources and detectors in the visible spectral region, would synergistically benefit large-scale production of low-cost plasmonic sensors in the visible spectral regions. For example, the sunlight can be used as a broadband light source and the human eye can be used as a detector for plasmonic sensing in the visible region.

In this article, we present a novel MDM structure that is easy to fabricate and has near-perfect absorption (> 99%) in the visible spectral region with an ultra-narrow bandwidth (~ 2 nm). Our focus is to investigate the position of plasmonic resonance wavelength and achieve near-perfect absorption of electromagnetic radiation in the spectral range of 200 to 800 nm. We observed that the variation in the refractive index of the dielectric layer, sandwiched between the gold grating and a gold film, and/or geometric parameters of the grating significantly affect the peak absorption and cause a redshift in the absorbance spectra of the proposed MDM structure. In this way, the proposed MDM structure offers flexibility to design a plasmonic metamaterial surface that can enable a perfect narrowband absorption at the desired wavelength in the visible. Owing to a narrow FWHM and only one rejection band for a broadband incidence light source, the proposed structure can be utilized as narrow-band rejection filters and plasmonic sensing applications. The absorption of the structure is calculated using the following formula:

$$A(\lambda) = 1 - R(\lambda) - T(\lambda) \quad (1)$$

where $T(\lambda)$ represents transmission through the structure as a function of wavelength. By making the bottom metal layer enough thick, the transmission of the metamaterials can be made to zero. So, the absorption calculation is done by using $A(\lambda) = 1 - R(\lambda)$. To achieve a perfect light absorption, the value of $R(\lambda) \approx 0$, which is only possible when the free space impedance matches with the effective impedance to satisfy the following criteria: $Z(\lambda) = \frac{\mu(\lambda)}{\epsilon(\lambda)}$.

Results and Discussion

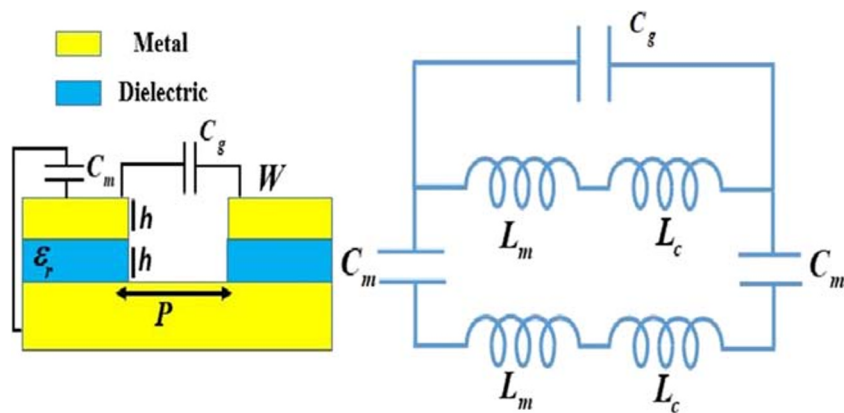
Equivalent Resonant LC Circuit

Figure 1 demonstrates the equivalent circuit model for the proposed absorber. The total impedance of the circuit can be expressed as:

$$Z_{total} = \frac{i\omega(L_m + L_e)}{1 - \omega^2 C_g(L_m + L_e)} - \frac{2i}{\omega C_m} + i\omega(L_m + L_e) \quad (2)$$

where $C_g = \frac{\epsilon_0 h}{p}$ is the gap capacitance, $C_m = \frac{C_1 \epsilon_0 \epsilon_r W}{h}$; here C_1 is a coefficient related to a non-uniform charge distribution at

Fig. 1 Schematics of the equivalent LC circuit model



the metal surface, $L_m = 0.5\mu_0Wh$, and $L_e = \frac{W}{r\epsilon_0h\omega_p^2}$, where r is a coefficient related to the effective cross-sectional area of metal, and ω_p is the plasma frequency of metal.

At resonance condition, $Z_{total} = 0$ $\omega = \frac{2\pi c_0}{\lambda}$ where c_0 is the speed of light in vacuum.

$$\lambda_r = 2\pi c_0 \left(\frac{C_m + C_g(L_m + L_e)}{C_m + C_g - \sqrt{C_m^2 + C_g^2}} \right)^{\frac{1}{2}} \tag{3}$$

For a large value of P , C_g is negligible resulting

$$\lambda_r = 2\pi c_0 \sqrt{C_m(L_m + L_e)} \tag{4}$$

For a large thickness of the dielectric layer, C_m is negligible over C_g that leads to

$$\lambda_r = 2\pi c_0 \sqrt{C_g(L_m + L_e)} \tag{5}$$

For the case when $C_m = C_g$, Eq. (3) can be simplified as

$$\lambda_r = 19.172\pi c_0 \sqrt{C_m(L_m + L_e)} \tag{6}$$

Design of Plasmonic System and FDTD Simulation

Figure 2a, b shows the perspective and schematic views of the proposed plasmonic structure. An array of a one-dimensional double-layered grating of metal and dielectric is designed on the gold film deposited on the SiO₂ substrate. Geometric parameters for the proposed plasmonic metamaterial structure are as follows: grating period (P), grating thickness (h_1 (gold) and h_2 (dielectric)), grating width (W_1 (gold), W_2 (dielectric)), H (gold layer thickness), and H' (substrate thickness). A finite difference time domain (FDTD) simulation software developed by Lumerical Solution Inc. was used for

the simulation of the proposed structure [31]. Lorentz-Drude material model was used to calculate the optical constants of Au [32]. Perfectly matched layer (PML) boundary conditions were used in the Y - and Z -directions, while periodic boundary condition was used in the X -direction. The interaction of incident electromagnetic radiation with the proposed structure can be understood using Maxwell’s curl equation written as follows:

$$\begin{aligned} \nabla \times \vec{H} &= \epsilon_0 \epsilon_r \frac{\partial \vec{E}}{\partial t} \\ \nabla \times \vec{E} &= -\mu_0 \frac{\partial \vec{H}}{\partial t} \end{aligned} \tag{7}$$

Where \vec{H} and \vec{E} represent magnetic and electric field respectively, ϵ_0 and μ_0 are permittivity and permeability of free space, respectively, and ϵ_r is the complex dielectric function.

After getting a numerical solution for the electric field \vec{E} and magnetic field \vec{H} from Eq. (2) using Yee’s algorithm of FDTD method, the spectral transmittance or reflectance of the proposed structure is solved using the following equation:

$$T_\lambda = \frac{\int S(x,y) dx dy}{Q_{\lambda,i}} \tag{8}$$

Here, Q corresponds to the incident power per unit area, and $S(x,y) = \frac{1}{T} \int_0^T \vec{E} \times \vec{H} dt$ is the Poynting vector time average and T is the period used in Eq. 2 to calculate the reflectance and transmittance.

To observe the influence of the refractive index of the dielectric grating, we calculated the absorption as a function of the dielectric grating index. The value of the index was numerically varied from 1.3 to 1.9 with a step of 0.1. The variations in the SPR peak position and peak absorbance with the refractive index of the dielectric layer are presented in Fig. 2c and d. Figure 2c shows a 2-D plot of

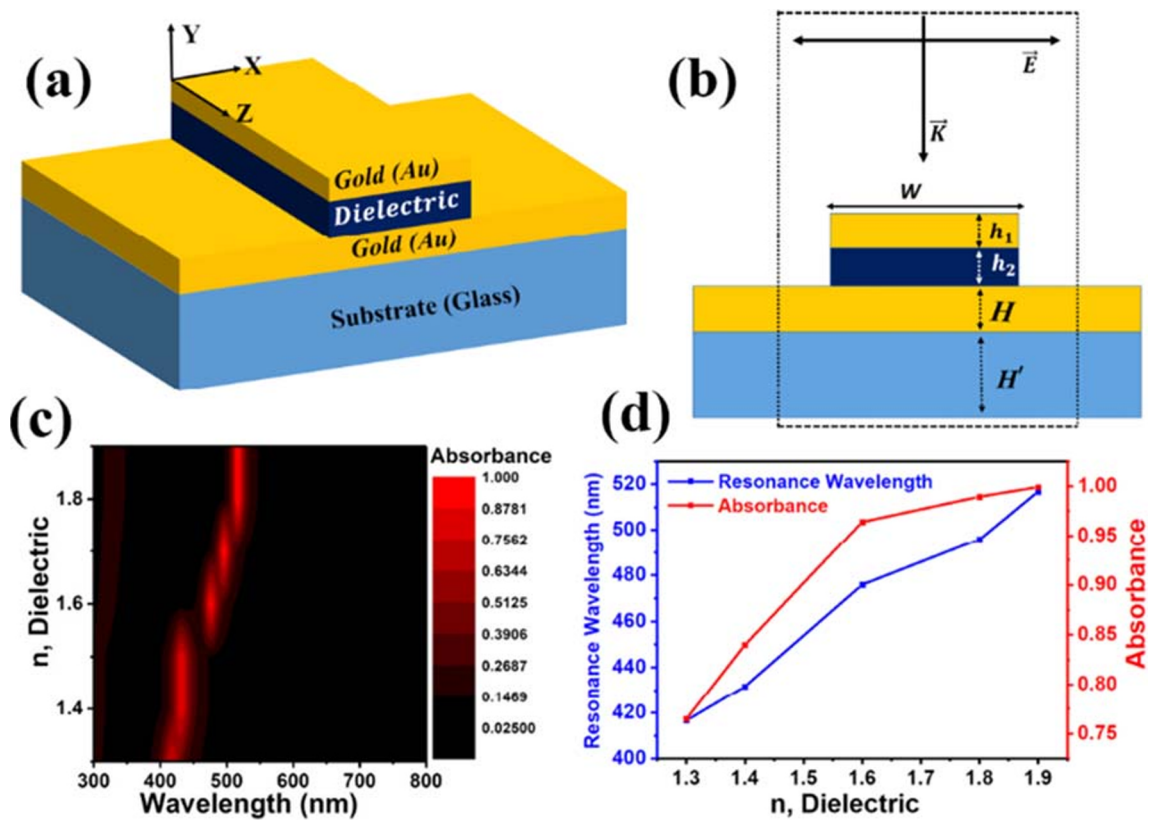


Fig. 2 3-D (a) and Schematic (b) views of proposed MDM plasmonic structure for one unit. Grating thickness h_1 (gold) and h_2 (dielectric) and grating width W_1 (gold) and W_2 (dielectric) are the variables with a fixed grating period of $P = 300$ nm. The dashed lines represent a unit cell of the periodic structure enclosing grating in the middle. The incident wave is

traveling \vec{k} in a negative Y -direction. The oscillation of the electric field \vec{E} is in the X -direction. **c** Absorbance as a function of grating refractive index and wavelength. **d** Variations in the resonance peak position and absorbance with the refractive index of the dielectric grating

absorption as a function of wavelength and grating refractive index. From Fig. 2c, one can observe a longer wavelength shift in the absorption peak position with an increase in the dielectric constant of the grating. From the LC model, presented in section II, an increase in the refractive index (n), and hence increase in the dielectric constant ($\epsilon_r = \epsilon_0 n^2$) of the dielectric material increases the value of the capacitance ($C_m = C_1 \epsilon_0 \epsilon_r W/h$) between two metal layers that increase the value of resonance peak position (λ_r) following the expression $\lambda_r = 2\pi c_0 \sqrt{C_m(L_m + L_e)}$ attributing to a longer wavelength shift. It reaches nearly 100% peak absorbance for the value of the refractive index of 1.9. Therefore, we can say that the designed structure works as a perfect narrowband absorber at resonance wavelength. Figure 2d shows variations in the position of resonance wavelength and absorbance with the refractive index of the dielectric grating. The shift in the resonance wavelength and absorbance for a unit change in the refractive index of the dielectric grating is around 20 nm/RIU and 7% RIU⁻¹ respectively. This variation can be seen from 1.3 to 1.8 and after 1.8 the shift

becomes almost saturated. The optimized result can guide one to choose a dielectric material for the proposed plasmonic system to attain nearly perfect narrowband absorption at the desired wavelength.

Optimization of Geometric Parameters

In this section, we will study the influence of different grating parameters on the optical response of the proposed MDM plasmonic structure. The geometric parameters are grating thickness (h_1, h_2), grating width (W_1, W_2), and grating period (P). The ratio of gold to dielectric grating thickness h ($\frac{h_1}{h_2}$) and the ratio of gold to dielectric grating width W ($\frac{W_1}{W_2}$) are fixed to the unit for the optimization. First of all, we optimized the values for h and W for a fixed grating period of $P = 300$ nm, $H = 250$ nm, and $H' = 300$ nm to achieve the best absorbance response of the proposed structure. After getting optimized grating thickness (h_1, h_2) and width (W_1, W_2), we performed an optimization for the grating period (P). The overall absorption

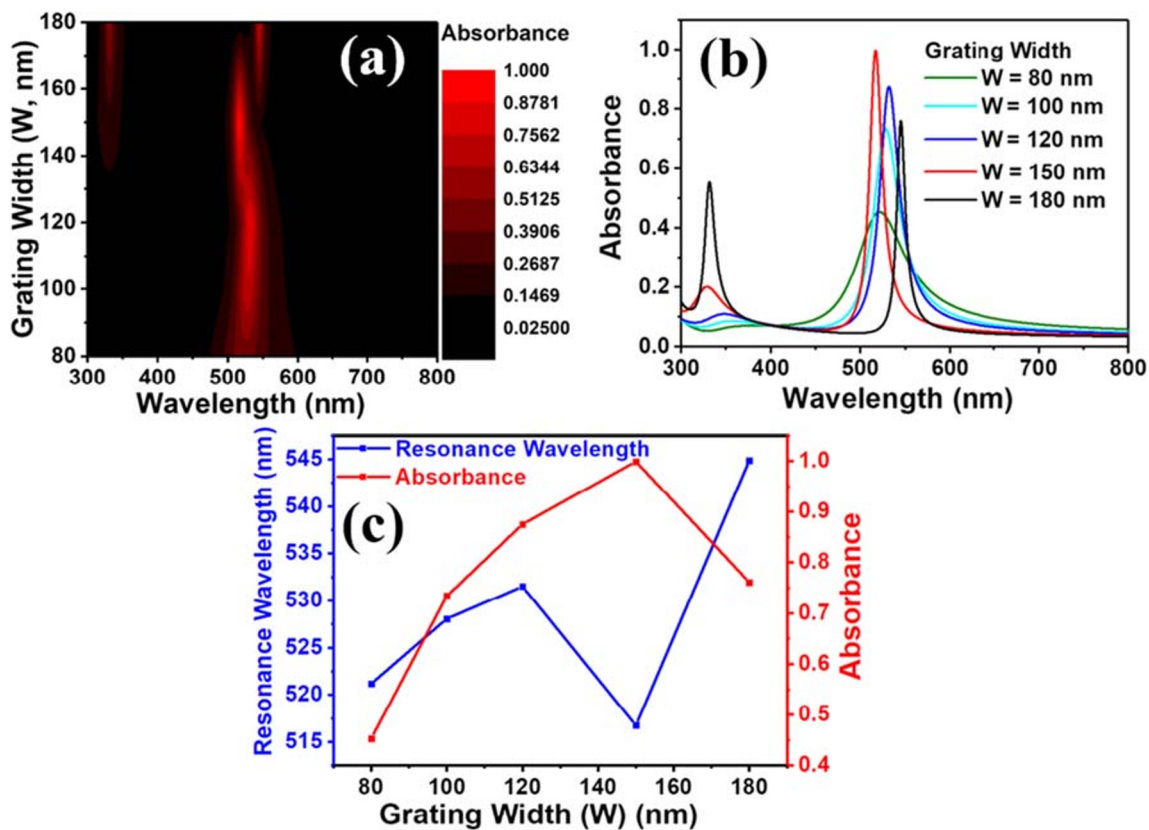


Fig. 3 Effect of grating width (W). **a** Absorbance contour plot **(b)** as a function of grating width and wavelength. **c** Absorbance intensity and resonance wavelength with grating width

in the proposed structure can be explained considering the equivalent LC circuit, as explained in the previous section. An increase in the width of the grating at a given period P increases the values of C_m , L_e , and L_m resulting in an increase in the value of resonance wavelength following Eqs. 3 to 6. Figure 3 shows the optical absorbance response of the proposed MDM structure with varying grating width, W , at $P = 300$ nm for 100 nm of h_1 and h_2 .

Figure 3a demonstrates a contour plot for absorbance as a function of grating width (W) and wavelength. From Fig. 3b, it is clear that the maximum absorption peak corresponds to $W = 150$ nm. Extracted resonance peak position and absorbance data for different grating widths are presented in Fig. 3c. The shift in the resonance wavelength and absorbance for grating width is $\sim 0.5\text{--}0.6$ nm/nm and $\sim 2\text{--}3\%$ / nm, respectively. From this optimization, we can see that $W = 150$ nm poses maximum absorbance and narrowest bandwidth; therefore, this grating width is chosen for the optimization of other geometric parameters.

Figure 4 shows the variation in the optical absorption response of the proposed plasmonic structure with grating thickness, h , for $P = 300$ nm with W_1 and W_2 equal to 150 nm. A significant red shift in the resonance

wavelength with a narrower FWHM is observed by either an increase in the grating thickness or an increase in the separation between the metal grating and metal film or both. According to the LC equivalent circuit theory, the top and bottom metallic layers are supporting antiparallel currents between two metallic films for the coupling of the magnetic field. Therefore, an increase in the thickness of the dielectric spacer between the metal film and metal grating affects the coupling strength of the magnetic field that increases the absorbance of electromagnetic radiation. An increase in the thickness of the dielectric layer decreases the value of C_m and increases the values of gap capacitance, C_g , and magnetic inductance L_m . Following expressions 3 to 6, an increase in the value of h results in a redshift in the resonance wavelength. The position of the resonance wavelength varies in the range of 380 to 680 nm by sweeping the grating thickness from 50 to 120 nm (Fig. 4a). The maximum absorption or coupling is observed for 100 nm thickness of the grating that corresponds to the resonance wavelength at 526 nm. It means that for an incident electromagnetic radiation of 526 nm wavelength, the proposed structure having a 100 nm thick, and 150-nm-wide grating with a grating period of

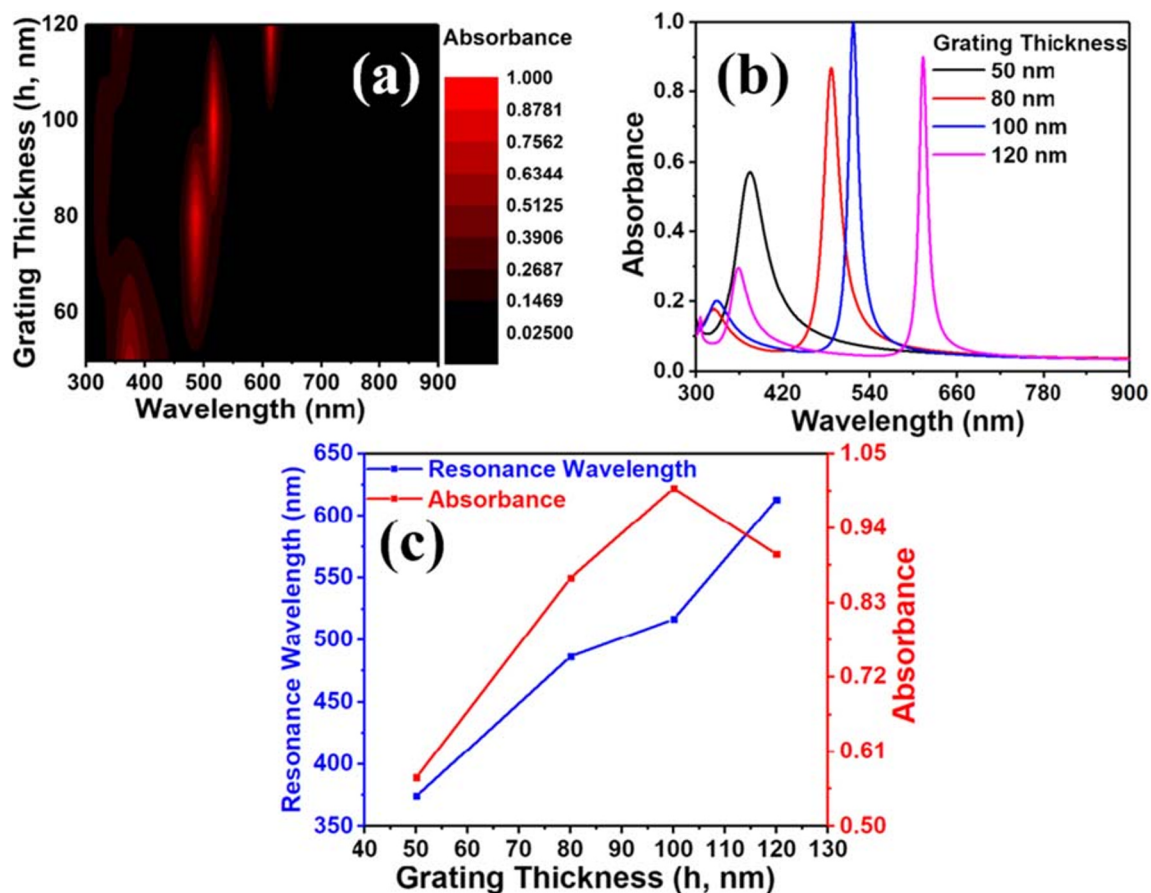


Fig. 4 Effect of grating thickness h . **a** Absorbance contour plot **(b)** as a function of grating thickness and wavelength. **c** Absorbance intensity and resonance wavelength with grating thickness

300 nm can offer a perfect impedance matching condition resulting in almost 100% optical absorption in a narrow spectral range. Figure 4b shows a 2-D plot of absorbance of the proposed structure as a function of its grating thickness and incident wavelength. The background response in all the cases is almost the same. The peak absorbance is close to one for the grating thickness of 100 nm. An increase or decrease in the grating thickness causes a decrease in the coupling strength resulting in a reduction in the peak absorbance. Figure 4c shows the rate of change in the resonance wavelength and peak absorbance with the grating thickness (h_1 and h_2). The changes in the resonance wavelength and peak absorbance with the grating thickness are around 30–40 nm/nm and 1–2%/nm, respectively.

After optimizing the grating width W (W_1 and W_2) and grating thickness h (h_1 and h_2), we also examined the effects of the grating period (P) on the optical absorption spectra of normally incident electromagnetic radiation. We can see that the position of peak absorption significantly depends on the grating period (Fig. 5a). With an increase in the grating period

from 270 to 360 nm, a redshift in the resonance peak is observed with a decrease in the peak absorbance. A contour plot for absorbance as a function of the grating period and wavelength is shown in Fig. 5a. Considering narrow linewidth, highest absorption, and strong coupling, we fix our grating period $\Lambda = 300$ nm. Figure 5c shows the rate of change of resonance wavelength and absorbance percentage with the grating period (P). The shift in the resonance wavelength and absorbance is around 0.1–0.2 nm/nm and 0.4–0.5%/nm, respectively. A small rate of change in the resonance peak position with the grating period can be explained with expression (4) of the LC model. An increase in the grating period decreases the value of gap capacitance C_g over C_m that makes resonance wavelength almost independent on the grating period.

We further characterize our structure by calculating its FWHM, dip strength, and figure-of-merit (FOM) as a function of the grating period, grating thickness, grating width, and index of the dielectric grating layer.

FOM can be calculated using the following relation, $\text{FOM} = \text{Peak absorbance}/\text{FWHM}$. The FWHM of resonance

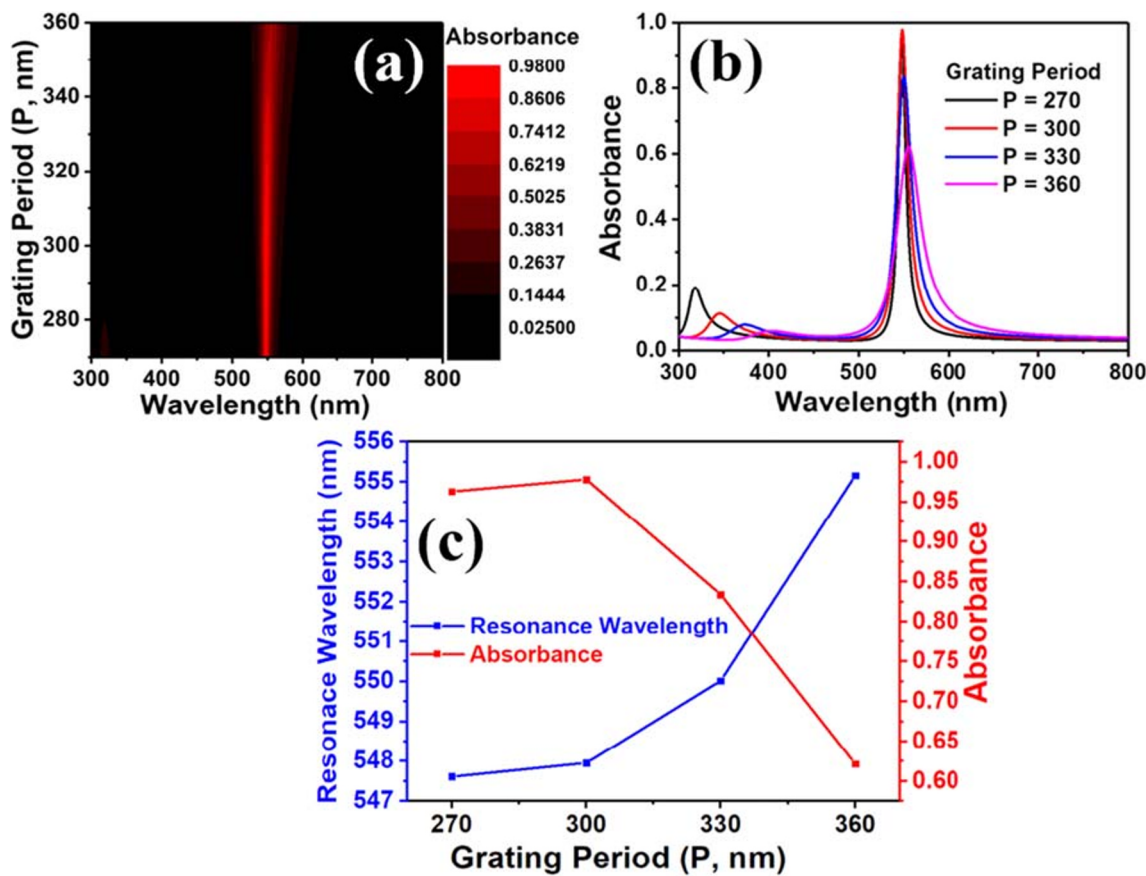


Fig. 5 Effect of grating period (*P*). **a** Absorbance contour plot **(b)** as a function of grating period and wavelength. **c** Absorbance intensity and resonance wavelength with grating period

absorption peak results in the accuracy of the SPR curve. A large value of FOM and a small value of FWHM are required for the high performance of a plasmonic sensor. From Fig. 6, we can see that the maximum FOM and minimum FWHM values are obtained corresponding to the following geometric parameters of the proposed plasmonic structure: grating period = 300 nm, grating thickness = 100 nm, grating width = 150 nm, and refractive index of the dielectric layer = 1.9.

Figure 7a shows the spectral absorption of the optimized proposed structure with nearly perfect absorbance in a narrow FWHM of 2.8 nm. To realize the mechanism responsible for this strong optical absorption in the proposed structure, we further investigated field and power distributions in the resonator. When the free space impedance is equal to the impedance of resonator, the incident electromagnetic energy fully gets converted into ohmic losses in the absorptive layer to accomplish the condition for perfect light absorption. The electromagnetic power absorbed in a non-magnetic material can be expressed as follows:

$$P_{abs} = \frac{1}{2} \omega \epsilon'' |E|^2 \tag{10}$$

where ω and ϵ'' are angular frequency and imaginary part of permittivity and $|E|$ is the total electric field confined in the material. As can be seen from Fig. 7c, d, most of the incident energy gets dissipated into the gold film due to the ohmic losses generated through SPR at resonance wavelength. The electric field gets confined at the interface and corners of the gold grating (Fig. 7c). Since the incident light is propagating along the *Y*-direction with polarization along the *X*-direction, therefore, the *X* component of the dipole moment is dominating. Figure 7b shows the effect of change in the incidence angle of electromagnetic radiation from 0° (normal incidence) to 40° with an increment of 0.50°. The calculated absorbance is outlined in Fig. 7b. The position of the surface plasmon resonance and peak absorbance is almost invariant with the incident angle.

Glucose Concentration Detection

The proposed MDM structure can be used for the fabrication of low-cost plasmonic sensors due to its ability to detect the change in the refractive index at the metal-dielectric interface.

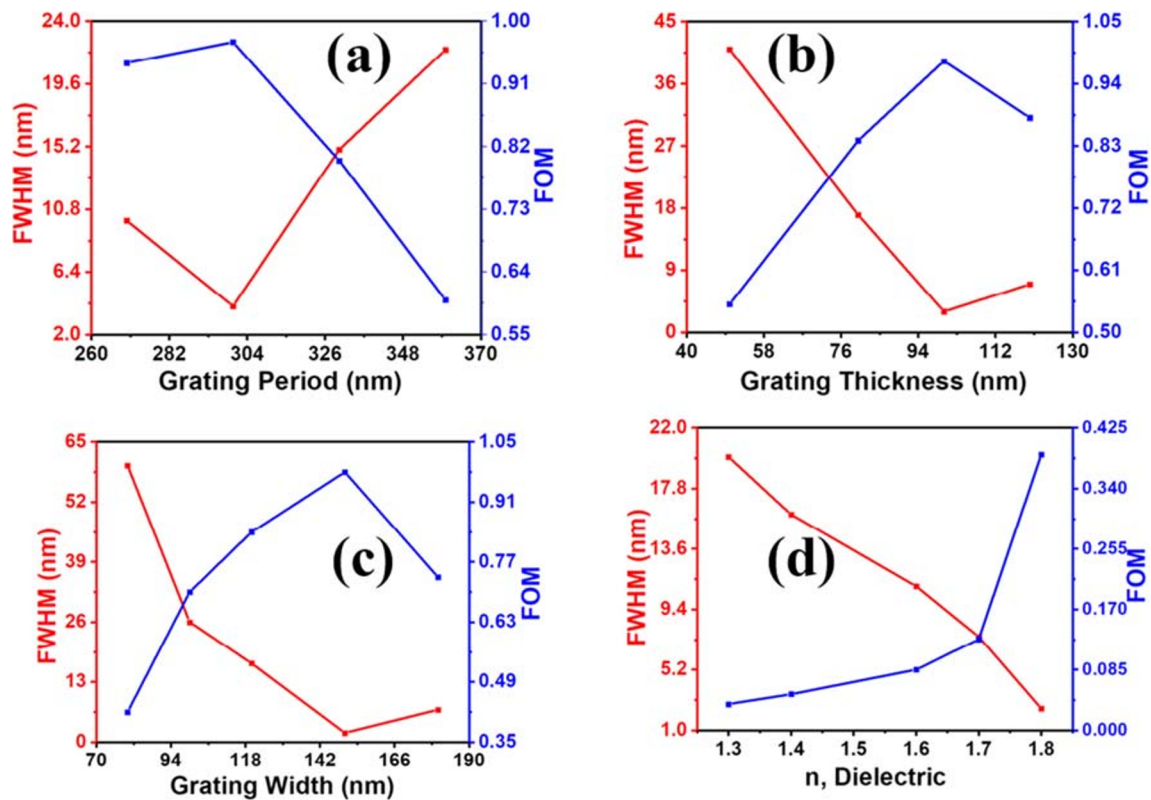


Fig. 6 Variation of FWHM and FOM as a function of grating period (a), grating thickness (b), and grating width (c). Refractive index of the dielectric layer (d)

SPR-based sensors can be used to detect a low concentration of gases in the air or small concentrations of biomolecules in the water such as blood group and DNA [33, 34]. Water is a significant ingredient of interstitial and intercellular liquids and the most important fluid in the living organisms. In this section, we will further study the response of the proposed structure for the detection of glucose concentration in water. As the refractive index of each biological sample is specific [35], this motivates research to form a mathematical approach to calculate the refractive index of different concentrations of glucose in water.

We used an established method called refractometric for the determination of sugar concentration in water. In this method, the refractive index of different known concentrations of a solute, in a given solvent, is first measured to draw a line-of-calibration, and then the line-of-calibration is used to determine the concentration of the unknown amount of solute in a solution from its measured refractive index. An increase in sugar concentration causes a corresponding increase in its refractive index. The following expression calculates the refractive index of any given aqueous solution of carbohydrate: $n = nW + aC$; here nW stands for the refractive index of water at room temperature and atmospheric pressure and $a =$

0.00143 is a coefficient representing the rate of change in the refractive index (n) of a solution with sugar concentration (C ; g/100 ml). Figure 8 shows the variation in the refractive index of the glucose solution with the concentration of sugar. The relation between the glucose concentration and refractive index shows that the refractive index of glucose solution varies linearly with the glucose concentration.

The variation in the refractive index of a solution with glucose concentration varies with the glucose concentration in water; therefore, the SPR curves corresponding to different glucose concentrations are also different. The reflectance and absorbance spectra for the proposed structure at different glucose concentrations are shown in Fig. 9a and b, respectively. A redshift in the resonance peak position can be seen with increasing glucose concentrations. The resonance wavelength peak position for the structure covered with different concentrations of glucose in 100 ml of water is shown in Fig. 9c along with corresponding values of refractive indices. Figure 9d represents the dynamic sensitivity $[S = \left(\frac{\partial \lambda}{\partial n} \right)_{n_0}]$, sensitivity at a given refractive index, of the structure extracted

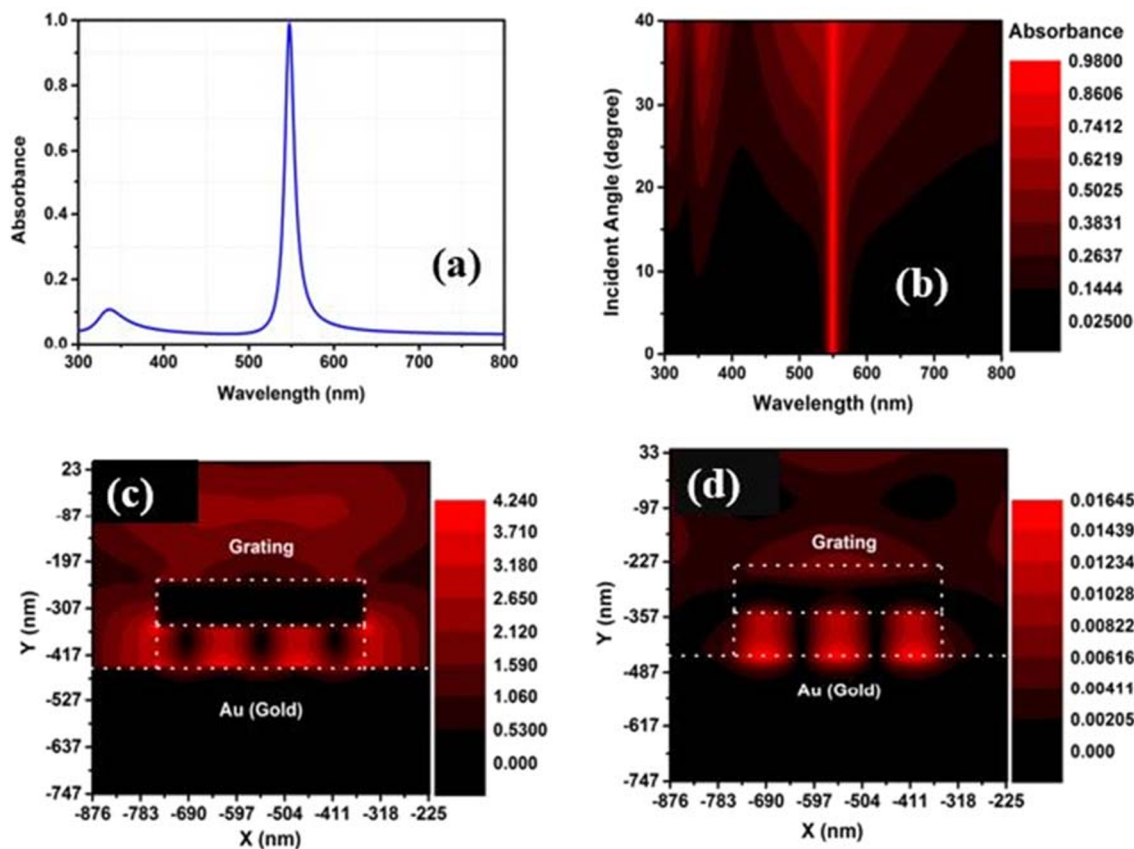


Fig. 7 a Absorbance for optimized geometry. b Effect of incidence angle increment on absorbance. Electric (c) and magnetic field (d) distribution at resonance wavelength, with $t = 100$ nm, $W = 150$ nm, and $\Lambda = 300$ nm

from Fig. 9c. The ratio of the shift in the resonance wavelength ($\partial\lambda$) with the change in the refractive index

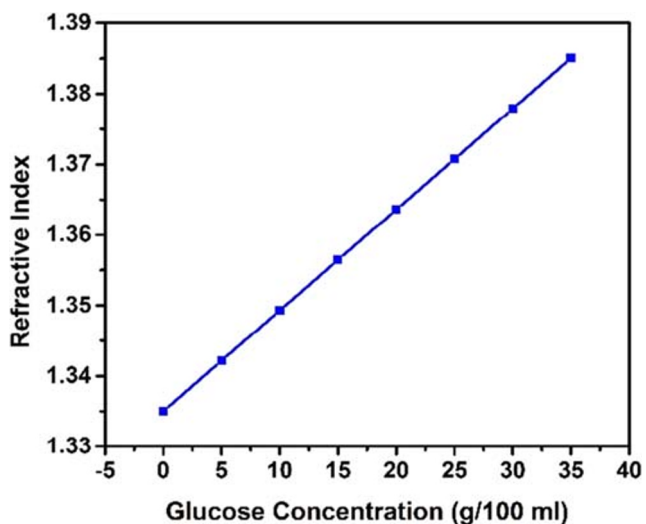


Fig. 8 Refractive index of the aqueous solution of glucose versus glucose concentration

(∂n) for an increase in the glucose concentration by 5 g in 100-ml solution is plotted with the corresponding value of the initial refractive index (n_0). The sensitivity of the structure dynamically increases from 140 to 195 nm/RIU with an increase in the refractive index from 1.33 to 1.38, i.e., change in the glucose concentration from 0 to 35 g/100 ml. We can also calculate the quality factor (χ) and figure of merit (FOM) of the plasmonic structure, against glucose sensing, using the following expression:

$$\chi = \frac{\text{Sensitivity}}{\text{FWHM}} \tag{11}$$

$$\text{FOM} = \frac{\text{Peak absorbance}}{\text{FWHM}} \tag{12}$$

Figure 10a represents variation in the QF (left) and FOM (right) of the designed plasmonic sensor with the

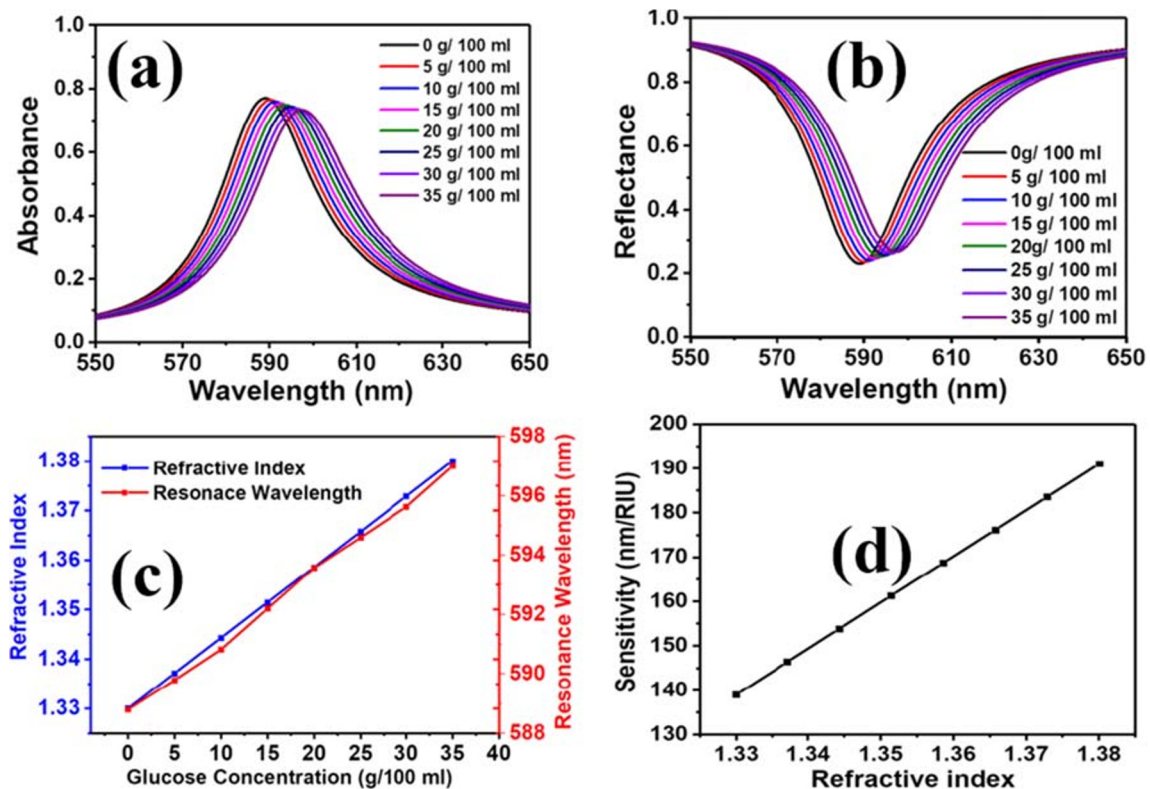


Fig. 9 **a** Absorbance for different glucose concentration. **b** Reflectance for different glucose concentrations. **c** Glucose concentration versus refractive index (left) and corresponding resonance wavelength (right). **d** Sensitivity

glucose concentration. The FOM values (Fig. 10a, red curve) are obtained using resonant absorbance (Fig. 10b) and corresponding FWHM values, extracted from Fig. 9a.

Plasmonic sensors can be realized using two strategies. In the first one, a broadband light source and a spectrometer are required to measure the shift in the resonance absorption peak position with the change in the ambient refractive index. In the second, and much simpler case, a monochromatic light source or a broadband light source coupled with a narrow bandpass filter and a photodetector are required. The intensity of the reflected light, at a wavelength close to the resonance absorption, is measured with the change in the ambient refractive index. The change in the SPR characteristics (peak position and FWHM) of the plasmonic structure with the ambient refractive index changes reflectance of the light close to the resonance wavelength. As can be seen from Fig. 10c, the reflectance of the designed plasmonic structure, at 596 nm, increases from 0.41 to 0.56 with an increase in the glucose concentration from 0 to 35 g/100 ml (i.e., $\Delta n = \sim 0.05$) resulting in a sensitivity ($S = \frac{\Delta R/R_0}{\Delta n/n_0}$, where R_0 and n_0 are reflectance and refractive index of the plasmonic structure with pure water) of ~ 9.6 arb. unit/ RIU.

Conclusion

In summary, we numerically designed and proposed a novel metal-dielectric-metal (MDM) structure that is easy to fabricate and has near-perfect absorption ($> 99\%$) in the visible spectral region with an ultra-narrow bandwidth (~ 2.8 nm) and its application in glucose detection. The proposed structure consists of a 1-D grating of gold on the top of a dielectric layer on a gold film. Optimization for dielectric grating index (n), grating thickness (t), grating width (W), and grating period (P) has been done to improve the performance of plasmonic structure by calculating its quality factor and figure-of-merit (FOM). We carried out our study on each and every factor that can influence the absorbance response of the proposed structure. Our study suggests that all the factors affect the resonance wavelength strongly and cause redshift with varying geometrical parameters. In a nutshell, we can say that the proposed plasmonic structure can be potentially reliable to be used for a particular application taking advantage of its varying resonance wavelength with almost the same background response. Due to this very narrow linewidth and possessing only one rejection band, it can also be utilized for filtering and different sensing applications. At the end, the optimized structure is tested for glucose sensing applications

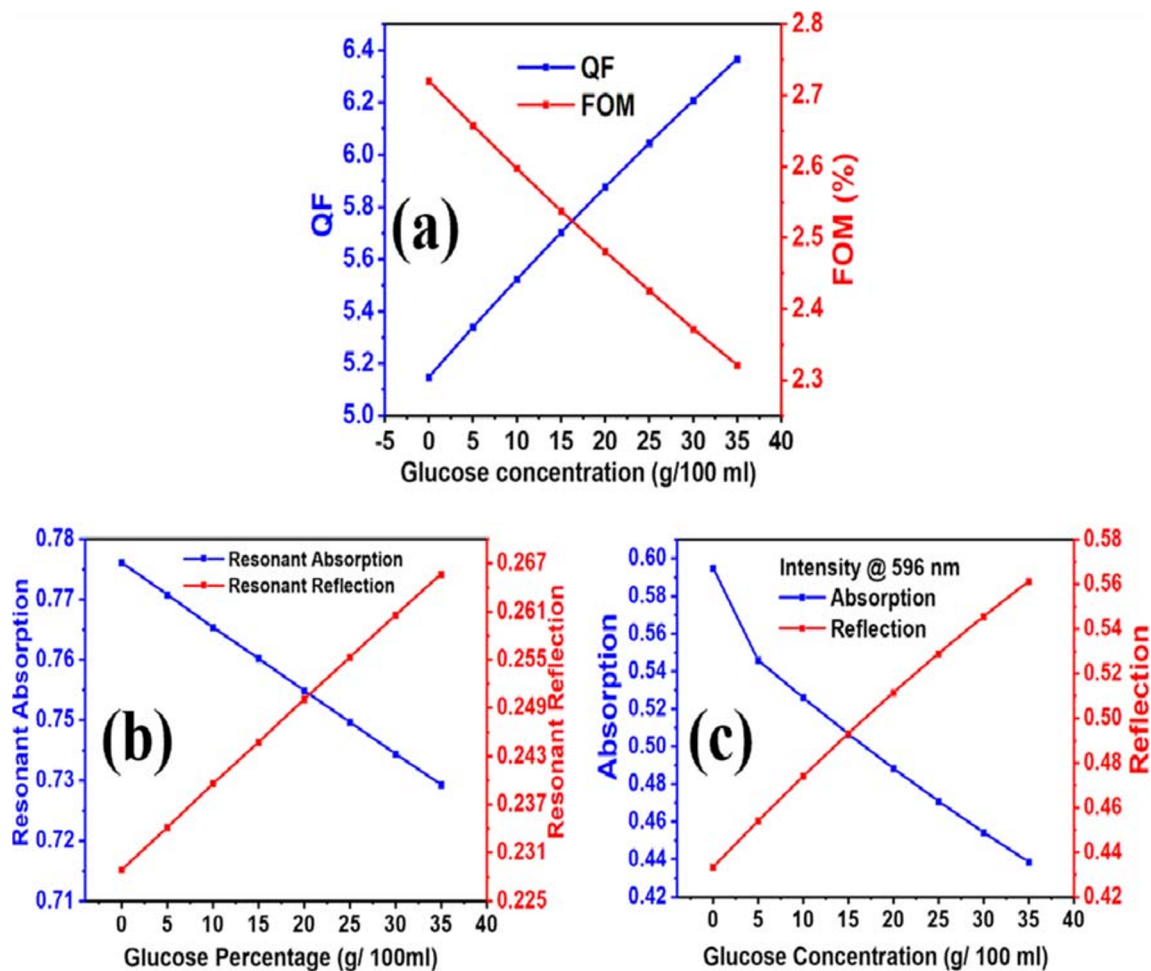


Fig. 10 **a** Glucose concentration versus quality factor (QF) (left) and figure-of-merit (FOM) (right). **b** Resonant reflection (right) and absorption (left) with the glucose concentration, and change in the reflection (right) and absorption (left) at 596 nm wavelength (**c**)

with dynamic sensitivity in the range of 140 to 195 nm/RIU for the shift in the resonance wavelength–based sensing and ~ 9.6 arb. unit/RIU for the sensor based on the change in reflectance at a given wavelength close to the resonance wavelength.

Acknowledgments The first author gratefully acknowledges his sponsorship by “CAS-TWAS Presidential’s Fellowship for international doctorate students.”

Funding information This work was supported in part by the National Key R&D Program of China (2017YFB1104700); National Natural Science Foundation of China (11674178); and Jilin Provincial Science & Technology Development Project (20180414019GH).

References

- Zheludev NI (2010) The road ahead for metamaterials. *Science* 328:582–583
- Wang B, Singh SC, Lu H, Guo C (2019) Design of aluminum bowtie nanoantenna array with geometrical control to tune LSPR from UV to near-IR for optical sensing. *Plasmonics*. <https://doi.org/10.1007/s11468-019-01071-z>
- Hao J (2011) Nearly total absorption of light and heat generation by plasmonic metamaterials. *Phys Rev B Condens Matter* 83:5919–5926
- Zhang J, ElKabbash M, Wei R, Singh SC, Lam B, Guo C (2019) Plasmonic metasurfaces with 42.3% transmission efficiency in the visible. *Light Sci Appl* 8(53)
- Chu D, Singh SC, Zhan Z, Sun X, Duan JA, Guo C (2019) Creation of enhanced transmission for clear and frosted glass through facile surface texturing. *Opt Mater Express* 9:2946–2954
- Yao C, Singh SC, ElKabbash M, Zhang J, Lu H (2019) Quasi-rhombus metasurfaces as multimode interference couplers for controlling the propagation of modes in dielectric-loaded waveguides. *Opt Lett* 44(7):1654–1657
- Ozbay E (2006) Plasmonics: merging photonics and electronics at nanoscale dimensions. *Science* 311:189–193
- Luk’yanchuk B, Zheludev NI, Maier SA, Halas NJ, Nordlander P, Giessen H, Chong CT (2010) The Fano resonance in plasmonic nanostructures and metamaterials. *Nat Mater* 9:707
- Plum E, Ou JY, Jiang L, Zheludev NI (2011) Reconfigurable photonic metamaterials. *Nano Lett* 11:2142–2144

10. Hayden O, Agarwal R, Lieber CM (2006) Nanoscale avalanche photodiodes for highly sensitive and spatially resolved photon detection. *Nat Mater* 5:352–356
11. Gu Y, Kwak ES, Lensch JL, Allen JE (2005) Near-field scanning photocurrent microscopy of a nanowire photodetector. *Appl Phys Lett* 87:1455
12. Liu X, Starr T, Starr AF, Padilla WJ (2010) Infrared spatial and frequency selective metamaterial with near-unity absorbance. *Phys Rev Lett* 104:207403
13. Richards PL (1994) Bolometers for infrared and millimeter waves. *J Appl Phys* 76:1–24
14. Singh SC, Peng Y, Rutledge J, Guo C (2019) Photothermal and Joule-heating-induced negative-photoconductivity-based ultrasensitive and near-zero-biased copper selenide photodetectors. *ACS Appl Electron Mater* 7:1169–1178
15. Jalil SA, Lai B, ElKabbash M, Zhang J, Garcell EM, Singh S, Guo C (2020) Spectral absorption control of femtosecond laser-treated metals and application in solar-thermal devices. *Light Sci Appl* 9(1):1–9
16. Aydin K et al (2011) Broadband polarization-independent resonant light absorption using ultrathin plasmonic super absorbers. *Nat Commun* 2:ncomms1528
17. Ding F et al (2014) Ultrabroadband strong light absorption based on thin multilayered metamaterials. *Laser Photonics Rev* 8(6):946–953
18. Wang B, Zhao C, Lu H, Zou T, Singh SC, Yu Z, Yao C, Zheng X, Xing J, Zou Y, Cunzhu Tong WEILIYU, Zhao B, Guo C Synergistic effects of electric-field-enhancement and charge-transfer based SERS study in AgS quantum dots/plasmonic bow-tie nanoantenna composite system. *Photonics Res.* <https://doi.org/10.1364/PRJ.383612>
19. Landy NI, Sajuyigbe S, Mock JJ, Smith DR, Padilla WJ (2008) Perfect metamaterial absorber. *Phys Rev Lett* 100:207402
20. Hu D, Wang H, Zhu Q (2016) Design of six-band terahertz perfect absorber using a simple U-shaped closed-ring resonator. *IEEE Photonics J* 8(2):1–8
21. Lee YP et al (2016) *Metamaterials for perfect absorption*, vol 236. Springer, Berlin
22. Chau Y-FC et al (2017) Simultaneous realization of high sensing sensitivity and tunability in plasmonic nanostructures arrays. *Sci Rep* 7(1):16817
23. Huang HJ et al (2017) Light energy transformation over a few nanometers. *J Phys D Appl Phys* 50(37):375601
24. Chau Y-FC et al (2018) Depolying tunable metal-shell/dielectric core nanorod arrays as the virtually perfect absorber in the near-infrared regime. *ACS Omega* 3(7):7508–7516
25. Yu P et al (2016) Dual-band absorber for multispectral plasmon-enhanced infrared photodetection. *J Phys D Appl Phys* 49(36):365101
26. Wang BX et al (2015) Design of a four-band and polarization-insensitive terahertz metamaterial absorber. *IEEE Photonics J* 7(1):1–8
27. Dayal G, Ramakrishna SA (2013) Design of multi-band metamaterial perfect absorbers with stacked metal–dielectric disks. *J Opt* 15(5):055106
28. Li R, Wu D, Liu Y, Yu L, Yu Z, Ye H (2017) Infrared plasmonic refractive index sensor with ultra-high figure of merit based on the optimized all-metal grating. *Nanoscale Res Lett* 12:1. <https://doi.org/10.1186/s11671-016-1773-2>
29. Hong JT, Jun SW, Cha SH, Park JY, Lee S, Shin GA, Ahn YH (2018) Enhanced sensitivity in THz plasmonic sensors with silver nanowires. *Sci Rep* 8, Article number: 15536
30. Singh SC, Zeng HB, Guo C et al (2012) *Lasers: fundamentals, types, and operations*. In: *Nanomaterials: processing and characterization with lasers*, 1st edn. Wiley, New York, pp 1–34
31. L. Inc. Lumerical Solutions, Inc. Retrieved <https://www.lumerical.com/products/fdtd-solutions/s>
32. Palik ED (1991) *Handbook of optical constants of solids II*, vol 1. Academic Press, Boston, pp 77–135
33. Rakhshani MR, Mansouri-Birjandi MA (2018) Engineering hexagonal array of nanoholes for high sensitivity biosensor and application for human blood group detection. *IEEE Trans Nanotechnol* 17:475–481
34. Sharma AK, Jha R, Pattanaik HS (2009) Design considerations for surface plasmon resonance-based fiber-optic detection of human blood group. *J Biomed Opt* 14:064041
35. Li H, Lin L, Xie S (2000) Refractive index of human whole blood with different types in the visible and near infrared ranges. *Proc SPIE* 3914:517–521

Publisher's Note Springer Nature remains neutral with regard to jurisdictional claims in published maps and institutional affiliations.